

NUMERICAL NS EQUATIONS-CONSTRAINED POWER OPTIMIZATION OF WIND TURBINES AFFECTED BY WAKE

YOUSEF AKHAVAN, MICHAEL CHEN, AND DONG LIANG*

Abstract. We develop a model for wind farm power optimization while considering the wake interaction among wind turbines. The proposed model is a Navier-Stokes equations-constrained optimization model with the objective of maximizing the total power where the operating points of the turbines are the decision variables, and the three-dimensional vorticity-velocity Navier-Stokes equations of wind speed are among the constraints. Moreover, we develop an efficient numerical algorithm to solve the optimization model. This algorithm is based on the pattern search method, the actuator line method and a time-stepping scheme which is used to solve the vorticity-velocity Navier-Stokes equations. In the numerical experiments, we first compute the power generation of a commercial wind turbine called WindSpot for different wind speed. It is shown that the computed power is in a good agreement with the measurements. Then, in the case of two turbines, we find that by optimizing the turbines' operation while considering the wake effect, we can gain an additional 8.11% in the total power when the incoming wind speed on the boundary is 10 m/s.

Key words. Wind farm power optimization, the vorticity-velocity Navier-Stokes equation, wake interaction, time-stepping, pattern search, optimization algorithm.

1. Introduction

Currently, wind turbines are operating at their own local optimum points to maximize their own performance. Many studies have shown that operating all turbines in a wind farm at their local optimum points leads to the suboptimal performance of the overall wind farm [1, 2]. This is due to the wake generated by upstream wind turbines which alter the flow field and lead to a wind velocity deficit in downstream wind turbines [3–5]. As a consequence, if all wind turbines operate at their own local optimum points then the downstream wind turbines cannot generate power as much as the upstream wind turbines. For instance, Neustadter and Spera [7] investigated the performance of three turbines separated by seven rotor diameters. They found that if all turbines operate at their own local optimum points then the power loss of downstream turbines can be as high as 10%. Another investigation by Rebecca [8] shows that the power loss of downstream wind turbines in full wake conditions can be as high as 30%, but when averaged over different wind directions, it is around 5–8%. These studies confirm that operating turbines at their local optimum points will lead to suboptimal performance of the overall wind farm. Therefore, in order to improve the performance of the overall wind farm, it is necessary to find the global optimum points of wind turbines by optimizing the total power while taking into account the impact of the wake on power production. In this regard, Patricio [9] studied the power optimization while considering the wake impact where the two-dimensional Navier-Stokes equations were used to model the airflow around turbines, where the study employed an inefficient grid search method to find optimum operating points of the upstream wind turbine while assuming that the downstream turbine is operating at its own local optimum points for the two

Received by the editors on March 7, 2024 and, accepted on November 30, 2024.
2000 *Mathematics Subject Classification.* 65N06, 65N12, 65M06, 65Y05.

*Corresponding author.

dimensional problem. There was no work on the realistic problems of the airflow around turbines in three dimensions modelled by three dimensional Navier-Stokes flow equations. In the framework of wind farm power optimization, in most of the studies, the total power is not explicitly optimized or the wake of wind turbines is modeled via an improvised BEM-alike method which has some limitations [7–11]. In these previous studies, there was few work to tackle the problem of explicitly optimizing the total power output in a wind farm. Thus, it is important to develop the wind power optimization where the total power will be explicitly optimized over multiple wind turbines in a wind farm.

In this paper, we develop a NS equations-constrained power optimization model over multiple wind turbines, for optimizing the total power output in a wind farm, by incorporating explicitly wake interactions among wind turbines. The important features are that the objective function of the total power is derived from the wakes of wind turbines by combining with the three dimensional vorticity-velocity Navier-Stokes equations as a constrain. The model optimizes on turbine operating while accounting for wake effects. It solves the optimization problem by embedding the three dimensional Navier-Stokes equations in the vorticity-velocity form with blade forces, which efficiently handles the wake effects in optimization. The proposed model is a PDE-constrained optimization model with the objective of maximizing the total power where the operating points of the turbines are the decision variables, and the constrained vorticity-velocity Navier-Stokes equations are used to compute the airflow as well as interacting wakes in the wind farm where the blade forces represent the loading of wind turbines. In the approach, a time-stepping finite difference scheme discretizes the three dimensional vorticity-velocity Navier-Stokes equations, where the false-transient technique ensures numerical stability, while the pattern-search derivative-free method is to solve the optimization procedure. The proposed algorithm of optimization approach is efficient and capable of handling the wind turbines in wind farms.

In numerical experiments, we first compute the power generation of a commercial wind turbine called WindSpot for different wind speed. It is shown that the computed power is in a good agreement with the measurements. We also show some numerical results that characterize the wake structure of the WindSpot. Furthermore, we find the global optimal operating points of multiple turbines operating in a wind farm. In the case of two turbines, we find that by optimizing the turbines' operation while considering the wake effect, we can gain an additional 8.11% in the total power when the incoming wind speed on the boundary is $10m/s$.

The paper is organized as the follows. In Section 2, we present the problem and the optimization model. In Section 3, we describe how to derive the aerodynamic forces using tabulated airfoil data. In Section 4, we present our numerical approach for solving the three-dimensional Navier-Stokes equations in the vorticity-velocity form. In Section 5, we describe the joint optimization algorithm for maximizing the total power production. In Section 6, we present the numerical case studies. Finally, conclusions are addressed in Section 7.

2. The Power Optimization Model in Wind Farm

For a wind farm with N turbines, the model for power optimization in its condensed form is as following

$$(1) \quad \begin{aligned} \text{Max}_{\substack{\beta_1, \beta_2, \dots, \beta_N \\ \Omega_1, \Omega_2, \dots, \Omega_N}} G_{TotalPower}(\mathbf{P}) &= \text{Max}_{\substack{\beta_1, \beta_2, \dots, \beta_N \\ \Omega_1, \Omega_2, \dots, \Omega_N}} \sum_{i=1}^N P_i \\ \text{Subject to Navier-Stokes equations: (3) - (7),} \\ \beta_{\min} \leq \beta_i \leq \beta_{\max}, \quad 1 \leq i \leq N, \\ \Omega_{\min} \leq \Omega_i \leq \Omega_{\max}, \quad 1 \leq i \leq N. \end{aligned}$$

Here, the decision variables are the rotational speed Ω_i and the pitch angle β_i of the i th turbine, for $i = 1, 2, \dots, N$. The parameters β_{\min} , β_{\max} , Ω_{\min} and Ω_{\max} are the physical limits of the adjustable pitch angle and the rotational speed.

The objective function of

$$(2) \quad G_{TotalPower}(\mathbf{P}) = \sum_{i=1}^N P_i$$

is to consider the total power generated in the wind farm, where P_i is the power generated by the i th wind turbine. The important function P_i , that describes the relationship of the power with wake of turbine, is developed as a nonlinear function of the direct decision variables, (24), by combining with other derived quantities from the Navier-Stokes equations (3)-(5). Due to its complexity, we derive the nonlinear function P_i , (24), in detail in Section 3.

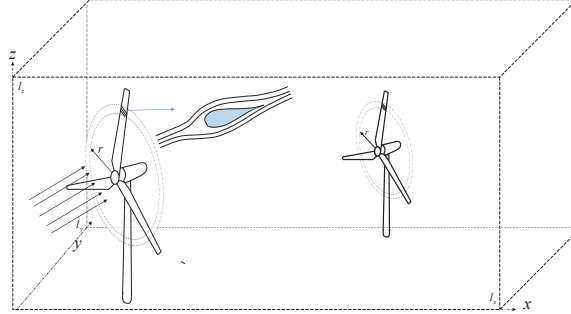


FIGURE 1. Computational domain.

For efficiently considering the relation to the total power and the wakes of wind turbines, we use the vorticity-velocity Navier-Stokes equations, where \mathbf{f}_ϵ is the loading of wind turbines. The constraint PDEs (3)-(7) are the three dimensional Navier-Stokes equations in the vorticity-velocity form, which are formulated by applying the curl operator on the Navier-Stokes equations in primitive variables. These equations on a rectangular domain, $D = [0, l_x] \times [0, l_y] \times [0, l_z]$ (see Figure 1), are given by

$$(3) \quad \frac{\partial \boldsymbol{\omega}}{\partial t} + \mathbf{U} \cdot \nabla \boldsymbol{\omega} = \boldsymbol{\omega} \cdot \nabla \mathbf{U} + \frac{1}{Re} \nabla^2 \boldsymbol{\omega} + \nabla \times \mathbf{f}_\epsilon,$$

$$(4) \quad \boldsymbol{\omega} = \nabla \times \mathbf{U},$$

$$(5) \quad \nabla \cdot \mathbf{U} = 0,$$

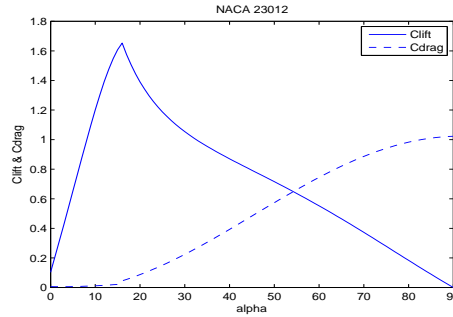


FIGURE 3. Lift and drag coefficients.

TABLE 1. NACA 23012 coefficients, $\alpha \in [0^\circ, 16^\circ]$.

	$C_L(\cdot)$	$C_D(\cdot)$
k_0	$1.0318e - 1$	$6.0387e - 3$
k_1	$1.0516e - 1$	$-3.6282e - 4$
k_2	$1.0483e - 3$	$5.4269e - 5$
k_3	$7.3487e - 6$	$6.5341e - 6$
k_4	$-6.5827e - 6$	$-2.8045e - 7$

and the angle of attack $\alpha(r)$, which is defined as the angle between the relative velocity and the chord line is:

$$(11) \quad \alpha(r) = \phi(r) - \beta(r),$$

where $\beta(r)$ is the local pitch angle. We remind that Ω and β are decision variables in the joint optimization model (1). The lift force $L(r)$, perpendicular to the relative wind direction, and the drag force $D(r)$ are:

$$(12) \quad L(r) = \frac{1}{2} \rho U_{rel}^2(r) c(r) b(r) C_L(\alpha(r)),$$

$$(13) \quad D(r) = \frac{1}{2} \rho U_{rel}^2(r) c(r) b(r) C_D(\alpha(r)),$$

where $c(\cdot)$ is the chord length of the airfoil and $b(\cdot)$ is the width of the blade section. In the above equations, $C_L(\cdot)$ and $C_D(\cdot)$ are the lift and drag coefficients at radius r which depend on the local angle of attack $\alpha(\cdot)$, see Figure 3. This figure shows the curves for the lift and the drag coefficients which are usually obtained by testing wing profiles in wind tunnels.

However, for numerical studies, it is convenient to have the curves as functions. For NACA 23012 profile [16] and for $0^\circ < \alpha(\cdot) < 16^\circ$, $C_L(\cdot)$ and $C_D(\cdot)$ are characterized by the following polynomial [21]

$$(14) \quad C_{L,D}(\alpha(r)) = k_0 + k_1 \alpha(r) + k_2 \alpha(r)^2 + k_3 \alpha(r)^3 + k_4 \alpha(r)^4,$$

where the polynomial coefficients are shown in Table 1. For an angle larger than the critical angle of attack, 16° , we apply the following corrections [21]

$$(15) \quad C_L(\alpha(r)) = A_1 \sin(2\alpha(r)) + A_2 \frac{\cos^2(\alpha(r))}{\sin(\alpha(r))},$$

$$(16) \quad C_D(\alpha(r)) = B_1 \sin^2(\alpha(r)) + B_2 \cos(\alpha(r)) + C_{Ds},$$

where

$$A_1 = \frac{B_1}{2}, \quad B_1 = C_{D,\max},$$

$$A_2 = (C_{Ls} - C_{D,\max} \sin(\alpha_{st}) \cos(\alpha_{st})) \frac{\sin(\alpha_{st})}{\cos^2(\alpha_{st})},$$

$$B_2 = \frac{1}{\cos(\alpha_{st})} (C_{Ds} - C_{D,\max} \sin^2(\alpha_{st})).$$

Here C_{Ls} and C_{Ds} are the lift and drag coefficients at stall angle of attack α_{st} , and $C_{D,\max}$ is the maximal value of the drag coefficient which is approximately 1, see Figure 3. We also need another correction due to the cross-flow effect at the blade tip. To take into account this effect, we employ the correction formulas

$$C_L(\cdot) = \frac{C_L(\cdot)}{F_{\text{corr}}}, \quad \text{and} \quad C_D(\cdot) = \frac{C_D(\cdot)}{F_{\text{corr}}(\cdot)},$$

where ([21])

$$(17) \quad F_{\text{corr}}(r) = \frac{2}{\pi} \arccos(\exp(-B \frac{R-r}{2r \sin(\phi(r))})).$$

In the above equation, B and R are the number of blades and the rotor radius, respectively. Now, we project the lift and drag force onto the axial and the tangential direction to get their components in these directions, from $L(r)$ and $D(r)$ in (12) and (13), as

$$(18) \quad F_x(r) = L(r) \cos(\phi(r)) + D(r) \sin(\phi(r)),$$

$$(19) \quad F_y(r) = L(r) \sin(\phi(r)) - D(r) \cos(\phi(r)).$$

Consequently, for the i th turbine with B blades, the thrust force $dT_i(r)$, the torque $d\Psi_i(r)$ and the power $dP_i(r)$ are

$$(20) \quad dT_i(r) = F_x(r)Bdr,$$

$$(21) \quad d\Psi_i(r) = F_y(r)Bdr,$$

$$(22) \quad dP_i(r) = d\Psi_i(r)(\Omega r).$$

Here, $dT_i(r)$ is along axial direction, and it is used to compute the source term in x -direction in the Navier-Stokes equations (3). The torque $\Psi_i(r)$ is along the tangential direction, and one must project it onto y and z -direction to compute the source terms in y and z -direction in the Navier-Stokes equations (3). From the equation (22), the generated power for the i th turbine with blade length R is

$$(23) \quad P_i = \int_0^R dP(r) = \int_0^R F_y(r)B\Omega r dr.$$

Using equations (12) and (13), the power generated by the i th turbine is

$$(24) \quad P_i = \frac{\rho B \Omega}{2} \int_0^R \left[U_{rel}^2(r) c(r) b(r) \left(C_L(\alpha(r)) \sin(\phi(r)) - C_D(\alpha(r)) \cos(\phi(r)) \right) \right] r dr,$$

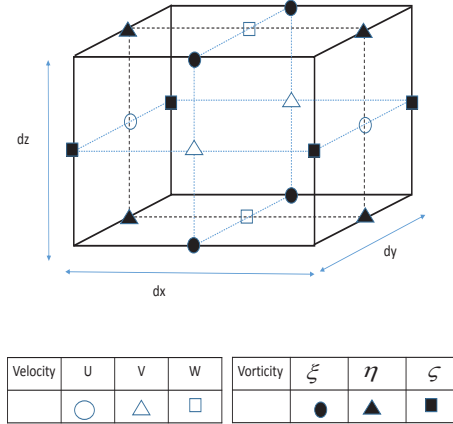


FIGURE 4. The staggered grid for the numerical scheme.

which is a function of Ω and $\alpha(r) = \phi(r) - \beta(r)$. Summing P_i from $i = 1$ to N will give the objective function of the optimization model (1),

$$(25) \quad G_{TotalPower}(\mathbf{P}) = \sum_{i=1}^N P_i,$$

which is the total power generated by all N turbines.

4. Numerical Method of Three Dimensional Vorticity-Velocity Navier-Stokes Equations

We seek numerical solutions to the three dimensional Navier-Stokes equations (3)-(5) in the vorticity-velocity form with blade forces. In order to ensure accuracy in the prediction of velocities and vorticities, a staggered grid system as displayed in Figure 4 is used in the present numerical scheme ([12]).

Let $U^n, V^n, W^n, \xi^n, \eta^n$ and ζ^n be the numerical approximations of U, V, W, ξ, η and ζ at time step n , then we solve the solution by the time-stepping procedure in the following steps.

1. The velocity Poisson equations, obtained as a result of taking curl of the vorticity, are made parabolic using the false-transient technique [13,14]

$$(26) \quad \alpha \frac{\partial \mathbf{U}^n}{\partial t} - \nabla^2 \mathbf{U}^n - \nabla \times \boldsymbol{\omega}^{n-1} = 0,$$

where α is a relaxation parameter. Central finite differencing scheme is used to approximate the second order derivatives that leads to a large linear system to be solved. Here, we use Generalized Minimum Residual technique to solve these linear systems but in a sparse format [15]. After we calculate velocities U and V using false transient method, then velocity W is calculated from the continuity equation as given below

$$(27) \quad \frac{\partial^2 W^n}{\partial z^2} = -\frac{\partial}{\partial z} \left(\frac{\partial U^n}{\partial x} + \frac{\partial V^n}{\partial y} \right).$$

Since the velocities U and V are already known, the resulting set of equations from (27) can be solved using the TDMA (Tridiagonal matrix algorithm).

2. The vorticity transport equations are discretized in time using the explicit scheme for the nonlinear term and implicit scheme for the linear term

$$(28) \quad \frac{\partial \boldsymbol{\omega}^n}{\partial t} + \mathbf{U}^n \cdot \nabla \boldsymbol{\omega}^{n-1} = \boldsymbol{\omega}^{n-1} \cdot \nabla \mathbf{U}^n + \frac{1}{Re} \nabla^2 \boldsymbol{\omega}^n + \nabla \times \mathbf{f}_\epsilon.$$

The central finite differencing scheme is used to approximate the first and second derivatives which leads to a large linear system, and it is solved by the generalized minimum residual technique. In the equation (28), the source term, $\mathbf{f}_\epsilon = (f_{\epsilon u}, f_{\epsilon v}, f_{\epsilon w})$ acts as a singular vorticity source along the rotor blades. To avoid singular behavior, \mathbf{f}_ϵ is formed by taking the convolution of the computed normal load, $\mathbf{f} = (f_u, f_v, f_w)$, and a regularization kernel, η_ϵ , as shown below [6]

$$(29) \quad \mathbf{f}_\epsilon = \mathbf{f} \otimes \eta_\epsilon,$$

where

$$(30) \quad \eta_\epsilon = \frac{1}{\epsilon^3 \pi^{\frac{3}{2}}} \exp\left(-\left(\frac{r}{\epsilon}\right)^2\right).$$

We remind the reader that f_u is computed directly using the equation (20). However, one needs to project the torque in the equation (21) which is along the tangential direction onto y and z -directions to compute f_v and f_w .

Finally, for a given pitch angle and rotational velocity, to compute U , V , W and \mathbf{f} simultaneously, we propose a time-stepping procedure which at every instant assures a time-true solution. This procedure is summarized in Algorithm 1.

Algorithm 1 Iterations between Navier-Stokes equations and blade Forces

- 1: for a given decision variables $\beta_i, \Omega_i, i = 1, 2, \dots, N$, let $x = [\beta_1, \beta_2, \dots, \beta_N, \Omega_1, \Omega_2, \dots, \Omega_N]^T$. For given boundary and initial conditions in (6) and (7) which indicates that the incoming wind speed is U_0 , let $n = 0$.
 - 2: **repeat**
 - 3: using U^n, V^n, W^n at the plane of wind turbines and the equations (8)-(24), compute the normal load of turbines \mathbf{f} as well as the power production of the turbines.
 - 4: calculate \mathbf{f}_ϵ using the computed normal load \mathbf{f} and the equation (29).
 - 5: using (26), (27) and (28), solve the Navier-Stokes equations (3)-(5) with the boundary and initial conditions given in (6) and (7) to get U^{n+1}, V^{n+1} and W^{n+1} .
 - 6: **until** steady-state solution is reached.
-

5. The Joint Optimization Algorithm

The objective function in (1) is the sum of the power produced by the individual turbines, P_i , which is given in the equation (24). From this equation, we note that P_i is a complicated nonlinear function of the direct decision variables as well as the wind speed at the plane of the rotor which is the solution of Navier-Stokes equations (3)-(5). Therefore, it is almost impossible to find the derivative of the objective function. Hence, we adopt the pattern search algorithm [17] which is a derivative

free method to solve the joint optimization model (1). For the model (1), let x be the vector of all decision variables and D_{feasible} be the feasible region

$$(31) \quad x \equiv [\beta_1, \beta_2, \dots, \beta_N, \Omega_1, \Omega_2, \dots, \Omega_N]^\tau,$$

$$(32) \quad D_{\text{feasible}} = \{x \mid \beta_{1\min} \leq x_1 \leq \beta_{1\max}, \dots, \Omega_{N\min} \leq x_{2N} \leq \Omega_{N\max}\},$$

and G be the objective function:

$$(33) \quad G \equiv \sum_{i=1}^N P_i,$$

then the joint optimization algorithm based on the pattern search method in its matrix notation is presented in Algorithm 2.

Algorithm 2 The Joint Numerical Optimization

- 1: initialize the parameters $\gamma_{\text{tol}}, \theta, \eta, \mu(\cdot)$, guess x_0 and set $\gamma_0 \geq \gamma_{\text{tol}}$.
 - 2: evaluate $G(x_0)$ by Algorithm 1 and (24).
 - 3: **for** $k = 1, 2, \dots, K$ **do**
 - 4: **if** $\gamma_k \leq \gamma_{\text{tol}}$ **then**
 - 5: return.
 - 6: **end if**
 - 7: **for** $p_k \in d$ **do**
 - 8: **if** $(x_k + \gamma_k p_k) \notin D_{\text{feasible}}$ **then**
 - 9: $x_k + \gamma_k p_k = x_b$.
 - 10: **end if**
 - 11: evaluate $G(x_k + \gamma_k p_k)$ by Algorithm 1 and (24).
 - 12: **if** $G(x_k + \gamma_k p_k) > G(x_k) + \mu(\gamma_k)$ **then**
 - 13: $x_{k+1} \leftarrow x_k + \gamma_k p_k$ and $\gamma_{k+1} \leftarrow \gamma_k \eta$.
 - 14: break.
 - 15: **else**
 - 16: $x_{k+1} \leftarrow x_k$ and $\gamma_{k+1} \leftarrow \gamma_k \theta$.
 - 17: **end if**
 - 18: **end for**
 - 19: **end for**
-

In Algorithm 2, x_b refers to the boundary point in the feasible search space. It is used when the step size and search direction take the solution outside the feasible region defined by the constraints on β and Ω . The parameters used in this algorithm are the convergence tolerance $\gamma_{\text{tol}} = 1e - 6$, the contraction parameter $\theta = 0.5$, the aggressive parameter $\eta = 2$, the sufficient increase function $\mu(s) = s^3/2$ and the direction set $d \equiv \{p_i, i = 1, 2, \dots, n+1\}$. In this direction set, the search directions are given by $p_i = \frac{1}{2n}E - E_i$, for $i = 1, 2, \dots, n$, and $p_{n+1} = \frac{1}{2n}E$, and E is the n dimensional vector of all ones and E_i is the i th column of the unit matrix of size n . Where n represents the number of decision variables (i.e., the pitch angle β and the rotational speed Ω). For a wind farm with N turbines, there are $2N$ decision variables, and we thus have $n = 2N$. Note that the search direction does not come from the gradient, but rather from a predetermined direction set d . Moreover, one member of d is a improving direction [17].

6. Numerical Experiments

6.1. Model Validation by Experimental Data. WindSpot is a $3.5kW$ three-bladed wind turbine with a rotor diameter of 4.05 meters. It can be fitted with different set of blades, essentially at zero twist angle with a active pitch control system. The chord length of this turbine is 0.254 meters at the hub, and it decreases linearly to 0.156 meters at the blade tip. Moreover, it is operating at a fixed rotational speed of $12 \frac{rad}{s}$ and a fixed pitch angle of 10.5 degrees [18]. To compute the flow field past the WindSpot, the computational domain is taken as $30m \times 14m \times 14m$ and the location of the wind turbine's hub is taken as $(10, 7, 7)$ in the domain. Moreover, the grid points are concentrated near the blade tips and stretched in the x , y and z -direction. The resulting grid consists of 46 grid points in the axial direction, 50 points in the y -direction and 57 points in the z -direction. In the axial direction the grid spacing ranges from $\Delta x = 0.02$ at the rotor plane to about $\Delta x = 1.9476$ in the far wake and in the y -direction the spacing takes values from $\Delta y = 0.02$ near the tip to about $\Delta y = 1.2150$ at the lateral boundary. Moreover, in the z -direction the spacing takes values from $\Delta z = 0.0346$ near the tip to about $\Delta z = 1.4863$ at the lateral boundary.

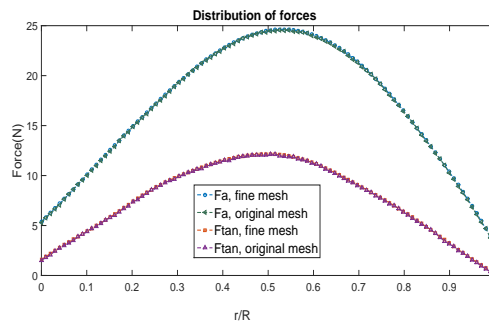


FIGURE 5. Comparison between forces on the fine mesh and original mesh.

In all the experiments, to ensure that the flow is fully developed in most of the wake, we solve Navier-Stokes equations with a time step of $\Delta t = 1e - 3$ until $t=10$ which corresponds to 10000 time steps. Moreover, the relaxation parameter in the equation (26) is taken as $\alpha = 1$ [19], the Reynolds number is taken as 10 and the constant which adjust the strength of the regularization function in the equation (30) is taken as $\epsilon = 0.03$ [20].

6.1.1. Influence of employed grid. To investigate the influence of the employed grid, we compute the distribution of the axial and tangential forces using a finer mesh which consist of $96 \times 100 \times 107$ grid points and the original mesh when the incoming wind speed is $U_0 = 10 \frac{m}{s}$. These distribution of the forces are displayed in Figure 5. From this figure, we can barely see the difference between forces in two computations. Therefore, the original grid is fine enough to ensure that the numerical results will be accurate.

6.1.2. Power generation of WindSpot. We now apply Algorithm 1 to estimate the power generation of WindSpot for different incoming wind speeds. The

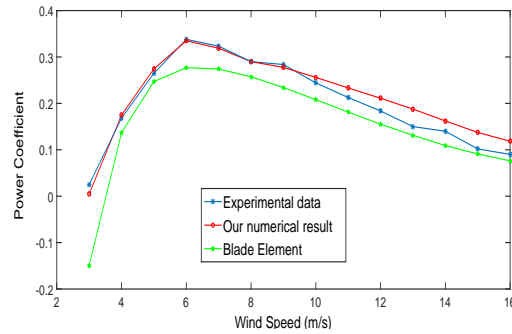


FIGURE 6. Comparison of measured and computed power.

numerical results are displayed in Figure 6. This figure shows the computed and the experimental power coefficient of WindSpot for different incoming wind speeds. From this figure, it is evident that the computed and measured values are in excellent agreement for wind speeds up to about $10 \frac{m}{s}$.

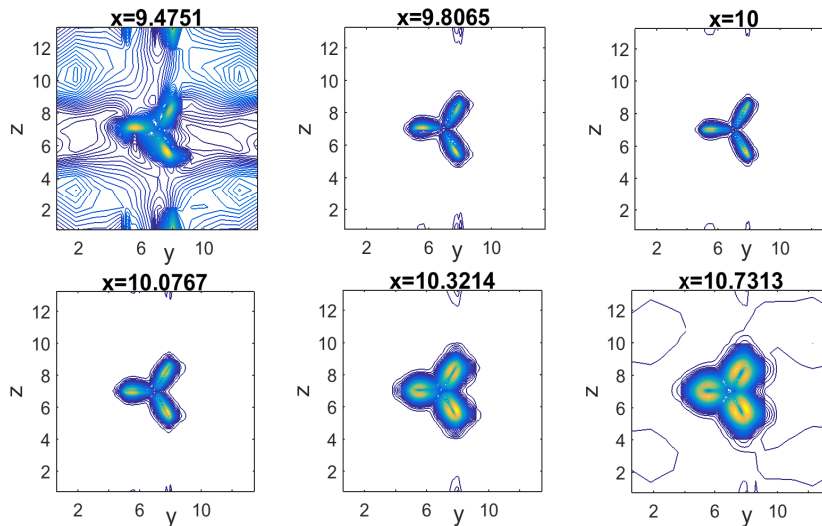


FIGURE 7. Computed magnitude of vorticity at the $y - z$ plane for $U_0 = 10 \frac{m}{s}$.

6.1.3. Wake structures. Here we investigate the wake structure of WindSpot when the incoming wind speed is $U_0 = 10 \frac{m}{s}$. The numerical results are displayed in Figures 7 and 8 which show the contours of magnitude of vorticity at $y - z$ planes in front of the turbine, at the plane of the turbine, at near wake and far wake. In these figures, the three blades are seen as lines with a high density of contour lines. Figure 8 shows the diffusion of the vortex about 3 to 4 rotor diameters behind the wind turbine. However, from experiments, it is known that the diffusion of the vortex happens at distance far behind the wind turbine [6]. This early diffusion of the vortex in our simulation which is explained by Sorensen in [6] is due to small Reynolds number and coarse grid used at far wake.

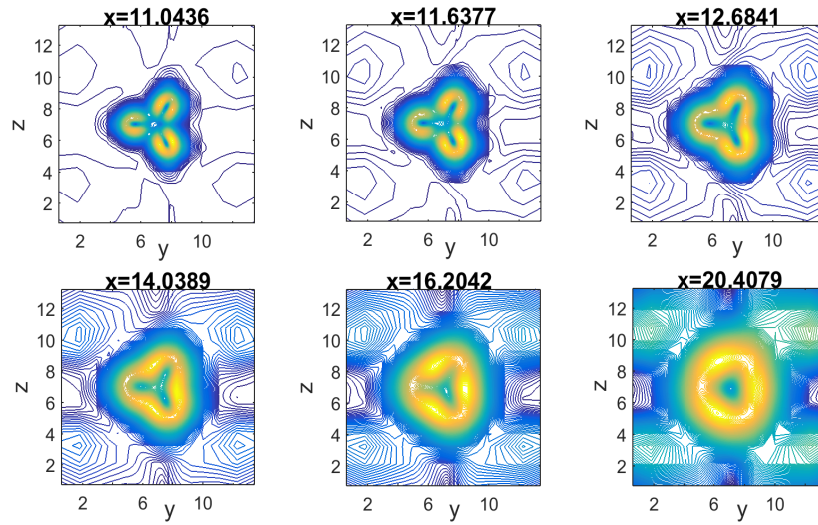


FIGURE 8. Computed magnitude of vorticity at the $y - z$ plane in near and far wake.

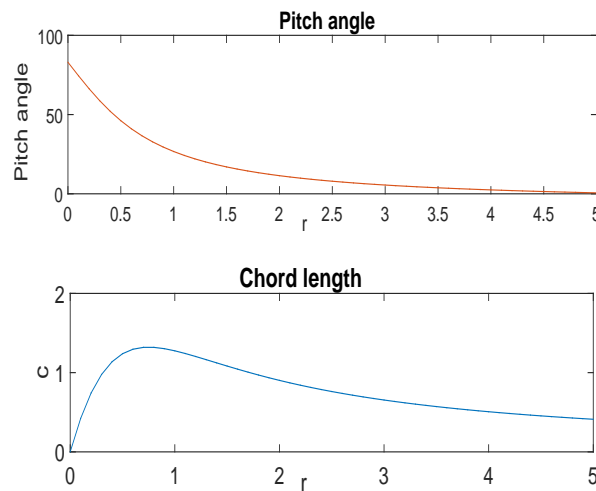


FIGURE 9. Chord length and pitch angle.

6.2. Power Optimization. In this section, we present two numerical case studies to test the efficiency and accuracy of the proposed numerical Algorithm 2. In these numerical case studies, we use a three-bladed wind turbine with a rotor diameter of 10 meters where the blade sections consist of NACA 23012 series airfoils. The chord length and the pitch angle as function of radius for this turbine are displayed in Figure 9 which are obtained using the Schmitz’s formula for the design of the optimal pitch angle and the chord length [21]. In both numerical case studies, the computations are carried out on a $100m \times 60m \times 60m$ computational domain. In the case of one turbine, the location of the hub is taken as $(20, 30, 30)$ and the case of two turbines the location of the hubs are taken as $(20, 30, 30)$ and $(60, 30, 30)$ for upstream and downstream turbines, respectively.

To capture the gradients of the flow field, grid points are concentrated near the blade tips and stretched in the axial direction as well as in the y and z -direction. In the case of one turbine, the resulting grid consists of 76 grid points in the axial direction, 80 points in the y -direction and 92 points in the z -direction. In the case of two turbines, the resulting grid consists of 96 grid points in the axial direction, 80 points in the y -direction and 92 points in the z -direction. In the axial direction, the grid spacing ranges from $\Delta x = 0.02$ at the rotor plane to about $\Delta x = 1.9476$ in the far wake and in the y -direction, the spacing takes values from $\Delta y = 0.02$ near the tip to about $\Delta y = 1.2150$ at the lateral boundary. Moreover, in the z -direction, the spacing takes values from $\Delta z = 0.0346$ near the tip to about $\Delta z = 1.4863$ at the lateral boundary.

6.2.1. Influence of employed grid. To investigate the influence of the employed grid, we compute the distribution of forces using finer meshes which consist of $126 \times 130 \times 142$ and $146 \times 130 \times 142$ grid points in the case of one and two turbines, respectively, and the original meshes when the incoming wind speed is $U_0 = 10 \frac{m}{s}$ and turbines are operating at their own local optimum points. These distribution of the forces are similar to the ones displayed in Figure 5 which indicate that the original grids for both cases are fine enough to ensure that the numerical results will be accurate.

TABLE 2. Optimal operating point of NACA 23012.

Wind speed	init.	β	Ω	α	T	Ψ	P
$U_0=9 \frac{m}{s}$	(-3, 2)	1.121	1.68	13.046	5.687	0.807	20.511
$U_0=10 \frac{m}{s}$	(1, 1.9)	1.375	1.800	13.187	6.545	1.010	30.006
$U_0=11 \frac{m}{s}$	(2, 1)	1.414	2.050	13.419	8.090	1.241	40.544

6.2.2. One turbine. We apply the developed numerical Algorithm 2 to find the optimal operating points of NACA 23012 when the incoming wind speed is $9 \frac{m}{s}$, $10 \frac{m}{s}$ and $11 \frac{m}{s}$. The results are tabulated in Table 2. From this table, the optimal pitch angle and the rotational speed are $\beta = 1.1215^\circ$ and $\Omega = 1.684 \text{ rad/s}$ when the incoming wind speed is $9 \frac{m}{s}$. At this optimal operating point, the generated power is $P = 20.5110 \text{ kw}$, the thrust is 5.6873 kilonewton, and the torque is 0.80744 kilonewton. These results are consistent with the field-tested results in [22]. Moreover, at this optimal operating point, the averaged angle of attack is $\alpha = 13.046^\circ$ which yields high glide ratio.

We now examine the performance of the developed numerical algorithm with different initial guesses. In this regard, we apply Algorithm 2 to find the optimal operating points of NACA 23012 using different initial guesses. The results are tabulated in Table 3. From this table, we observe that Algorithm 2 starting from the initial guesses $\beta_0 = 0^\circ$ and $\Omega_0 = 1 \text{ rad/s}$ finds the optimal solutions of $\beta = 1.1213^\circ$ and $\Omega = 1.6837 \text{ rad/s}$ when the incoming wind speed is $9 \frac{m}{s}$. The magnitude of difference between these optimal points and those optimal points associated with the incoming wind speed of $9 \frac{m}{s}$ in Table 2 is very small. The algorithm showed

consistency with respect to the two initial guesses tested. Moreover, these results imply that the optimal operating points of a free-standing turbine are unique.

TABLE 3. Optimal operating point of NACA 23012 (different initial point).

Wind speed	init.	β	Ω	α	T	Ψ	P
$U_0=9 \frac{m}{s}$	(0, 1)	1.121	1.683	13.046	5.687	0.807	20.511
$U_0=10 \frac{m}{s}$	(-2, 1)	1.375	1.802	13.188	6.545	1.010	30.006
$U_0=11 \frac{m}{s}$	(-2, 1.7)	1.416	2.055	13.412	8.090	1.240	40.543

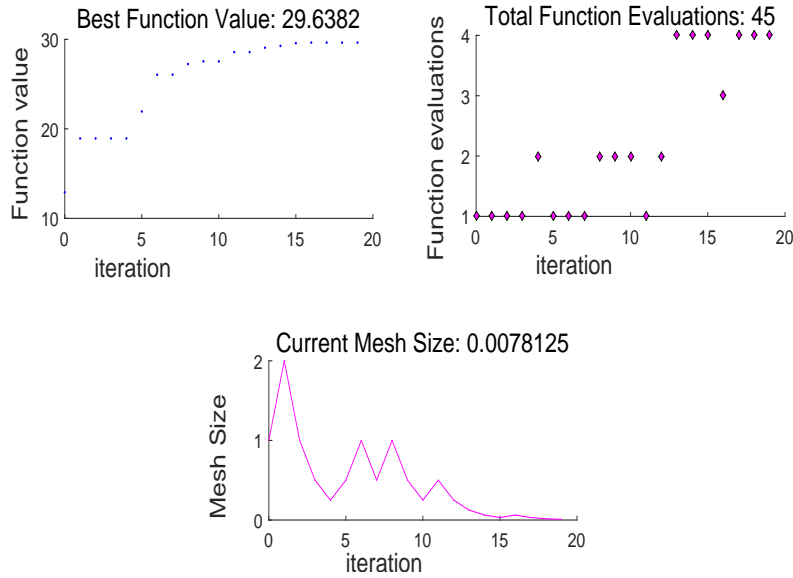


FIGURE 10. Pattern search results for the incoming wind speed $U_0 = 10$.

We also investigate the efficiency of the developed numerical algorithm in terms of the number of objective function evaluations required for our algorithm to reach convergence. In this regard, the best objective function value, the number of objective function evaluations and the mesh size at each iteration of Algorithm 2 are plotted for $U_0 = 10$ in Figure 10. From this figure, it is evident that Algorithm 2 converges to the stationary point 29.6382 as the sequence of the mesh size parameter tends to zero. From this figure, we also note that the number of objective function evaluations is 45. With this number of objective function evaluations, Algorithm 2 seems to find the optimal operating points of a single turbine in a reasonable time. However, as the number of turbine increases the objective function evaluation becomes substantially expensive. Therefore, for future work we are planning to develop a robust optimization algorithm to speed up the optimization process.

6.2.3. Two turbines. We now apply the developed numerical Algorithm 2 to find the global optimum operating point of two NACA 23012 which are four rotor diameters apart. The results are tabulated in Table 4. From this table, the global optimum point of upstream and downstream turbine are $(\beta, \Omega) = (1.1646, 1.5915)$ and $(\beta, \Omega) = (0.7470, 1.3086)$, respectively. Moreover, from this table, we also note that the upstream turbine generates 18.575 *kw* power and the downstream turbine generates 17.107 *kw* power when they operate at their global optimum point. In this case, the total power output of wind turbines is 35.682 *kw*. In contrast, when both turbines operate at their own optimum point, i.e., $(\beta, \Omega) = (1.1215, 1.6840)$, as shown in Table 2, then the upstream turbine generates 16.495 *kw* power and the downstream turbine generates 16.226 *kw* power. In this case, the total power output of wind turbines is 32.721 *kw*. Therefore, by optimizing the turbines' operation while considering the wake effect, we can gain an additional 9.05% in the total power when the incoming wind speed on the boundary is 9 *m/s*, since $35.682/32.721 = 1.0905$. Moreover, we also note that this extra gain in the total power does not lead to increased loading on wind turbines. For example, from Table 4, the thrust of the downstream turbine operating at its global optimum point and in the wake of upstream turbine is $T = 5.2265 *kN*$ which is less than the thrust of a free-standing turbine $T = 5.6873 *kN*$, see Table 2, operating at its own optimal point with no exposure to the wake of another turbine. Further, for the results related to other two incoming wind speeds 10 *m/s* and 11 *m/s* in Table 4, comparing with those in Table 2, we can see that by optimizing the turbines' operation, we can safely gain additional 8.11% in the total power when the incoming wind speed on the boundary is 10 *m/s* and additional 7.37% in the total power when the incoming wind speed on the boundary is 11 *m/s*.

TABLE 4. Joint optimal operating points of two NACA 23012.

Wind speed	turbine	β	Ω	α	T	Ψ	P
$U_0=9 \frac{m}{s}$	1st, joint	1.164	1.591	13.120	5.170	0.755	18.575
	2nd, joint	0.747	1.308	22.369	5.226	0.750	17.107
	1st	1.121	1.684	11.300	5.146	0.643	16.495
	2nd	1.121	1.684	11.163	5.118	0.629	16.226
					Gain:	9.04%	
$U_0=10 \frac{m}{s}$	1st, joint	0.597	1.525	15.186	6.348	0.985	26.879
	2nd, joint	0.082	1.393	18.151	6.391	0.965	25.835
	1st	1.375	1.800	11.459	5.945	0.815	24.520
	2nd	1.375	1.800	11.332	5.913	0.800	24.246
					Gain:	8.11%	
$U_0=11 \frac{m}{s}$	1st, joint	0.331	1.722	17.489	8.242	1.199	35.750
	2nd, joint	0.827	1.611	16.451	7.255	1.197	34.691
	1st	1.416	2.050	11.674	7.360	1.004	33.306
	2nd	1.416	2.050	11.551	7.323	0.986	32.860
					Gain:	7.37%	

From Table 2, we note that a free-standing wind turbine operating at its optimum point $(\beta, \Omega) = (1.1215, 1.6840)$ generates 20.5110 *kw* power when the incoming wind speed is 9 *m/s*. In contrast, if two turbines are grouped in a wind farm, and they operate at the optimum point of a free-standing turbine, then the upstream and downstream turbine generate 16.495 *kw* and 16.226 *kw* power, respectively. This power reduction of the downstream turbine is due to the wake generated by upstream wind turbine which alters the flow field and leads to a wind velocity deficit in the downstream wind turbine. The power reduction of the upstream wind turbine can be justified due to the thrust generated by the downstream turbine which

reacts to the common flow field, and leads to a wind velocity deficit in the upstream wind turbine. In this perspective, the wake zone concept could be extended. It is not only the turbine at front affects the performance of the turbines at rear; rather, all turbines affect each other via the common flow field in which they are immersed.

7. Conclusion

In this paper, we studied how to optimize power production of multiple wind turbines by considering the wake interactions among them. A NS equations-constrained power optimization model was developed for optimizing the total power output over wind turbines in a wind farm by incorporating explicitly wake interactions. We modeled the intricate interference of multiple turbines through the actuator line method and the three dimensional Navier-Stokes equations in the vorticity velocity form. We find that by optimizing the turbines' operation, we can safely gain an additional 8.11% in the total power when the incoming wind speed on the boundary is 10 m/s.

We find that not only the turbine at the front affects the production of a turbine at the rear, but all turbines affect each other by exerting forces into the flow field in which all turbines are immersed.

This work paves a way for a larger scale power production optimization and more accurate wind farm layout optimization.

Acknowledgments

The authors would like to thank the referees for their valuable comments which have helped to improve the paper greatly. This work was supported partially by Natural Sciences and Engineering Research Council of Canada.

References

- [1] Marden, J. R. and Ruben, S. and Pao, L., A model-free approach to wind farm control using game theoretic methods, *IEEE Transactions on Control Systems Technology*, 21 (2013), 1207-1214.
- [2] Johnson, K. E. and Thomas, N., Wind farm control: Addressing the aerodynamic interaction among wind turbines, *American Control Conference*, (2009), 2104-2109.
- [3] Shen, W. Z. and Sorensen, J. N. and Munduate, X., Analysis of wake states by a full-field actuator disc model, *Wind Energy*, 1 (1998), 73-88.
- [4] Crespo, A. and Vermeera, L. J. and Sorensen, J. N., Wind turbine wake aerodynamics, *Progress in Aerospace Sciences*, 39 (2003), 467-510.
- [5] Sanderse, B., Aerodynamics of wind turbine wakes literature review, *Energy Research Centre of the Netherlands*, 16 (2009).
- [6] Sorensen, J. N. and Shen, W. Z., Numerical Modeling of Wind Turbine Wakes, *Journal of Fluids Engineering*, 124 (2002), 393-399.
- [7] Neustadter, H. E. and Spera, D. A., Method for evaluating wind turbine wake effects on wind farm performance, *Journal of Solar Energy Engineering*, 107 (1985), 240-243.
- [8] Barthelmie, R. J. and Frandsen, S. T. and Hansen, K. and Schepers, J. G. and Rados, K. and Schlez, W. and Neubert, A. and Jensen, L. E. and Neckelmann, S., Modelling the impact of wakes on power output at Nysted and Horns Rev, *European Wind Energy Conference*, (2009).
- [9] Torres, P. and van Wingerden, J. W. and Verhaegen, M., Modeling of the flow in wind farms for total power optimization, *IEEE International Conference on Control and Automation*, (2011), 18-21.
- [10] Jin, Z. and Li, F. and Ma, X. and Djouadi, S., Semi-Definite Programming for Power Output Control in Wind Energy Conversion System, *IEEE Transactions on Sustainable Energy*, 5 (2014), 466-575.
- [11] Iov, F. and Hansen A. D. and Sorensen, P. and Blandjerg, F., Centralized power control of wind farm with doubly fed induction generators, *Renewable energy*, 31 (2006), 935-941.

- [12] Lo, D. C. and Murugesan, K. and Young, D. L., Numerical solutions of three-dimensional velocity-vorticity Navier-Stokes equations by finite difference method, *International Journal for Numerical Methods in Fluids*, Lo, D. C. and Murugesan, K. and Young, D. L., 147 (2005), 1469-1487.
- [13] Napolitano, M. and Pascazio, G., A numerical method for the vorticity-velocity Navier-Stokes equations in two and three dimensions, *Computer and Fluids*, 19 (1991), 489-495.
- [14] Guj, G. and Stella, F., Numerical solutions of the high-Re recirculating flows in vorticity-velocity form, *International Journal for Numerical Methods in Fluids*, 8 (1988), 405- 416.
- [15] Saad, Y., *Iterative Methods for Sparse Linear Systems*, PWS Publishing Company, Boston, (1996).
- [16] de Vries, O., *Fluid dynamic aspects of wind energy conversion*, Advisory Group For Aerospace Research and Development Neuilly-Seine (France), 1979.
- [17] Nocedal, J. and Wright, S. J., *Numerical Optimization*, Springer Series in Operations Research. New York: Springer-Verlag, (1999).
- [18] Liu, S. and Janajreh, I., Development and application of an improved blade element momentum method model on horizontal axis wind turbines , *International Journal of Energy and Environmental Engineering*, 3 (2012), 30.
- [19] Mallinson, G. D. and de Vahl Davis, G., The Method of the False Transient for the Solution of Coupled Elliptic Equations , *Journal of Computational Physics*, 12 (1973), 435-461.
- [20] Sorensen, J. N. and Shen, W. Z. and Munduate, X., Analysis of Wake States by a Full-field Actuator Disc Model, *Wind Energy*, 1 (1998), 73-88.
- [21] McCosker, J., Design and Optimization of a Small Wind Turbine, *Rensselaer Polytechnic Institute Hartford, Connecticut*, 3 (2012), 456-495.
- [22] Sorensen, J. N. and Kock, C. W., A model for Unsteady Rotor Aerodynamics, *Journal of Wind Engineering and Industrial Aerodynamics*, 58 (1995), 259-275.
- [23] Seguro, J. V. and Lambert, T. W., Modern estimation of the parameters of the Weibull wind speed distribution for wind energy analysis, *Journal of Wind Engineering and Industrial Aerodynamics*, 85 (2000), 15-84.
- [24] Manwell, J. F. and McGowan, J. G. and Rogers, A. L., *Wind energy explained: theory, design and application*, A John Wiley and Sons Ltd , (2009).
- [25] Jiang, B. N. and Lin, T. L. and Povinelli, L. A., Large-scale computation of incompressible viscous flow by least-squares finite element method, *Computer Methods in Applied Mechanics and Engineering*, 114 (1994), 213-231.
- [26] Tang, L. Q. and Cheng, T. and Tate, T. and Tsang, H., Transient solutions for three-dimensional lid-driven cavity flows by a least-squares finite element method, *International Journal for Numerical Methods in Fluids*, 21 (1995), 413-432.
- [27] Ho, C. J. and Lin, F. H., Numerical simulation of three-dimensional incompressible flow by a new formulation, *International Journal for Numerical Methods in Fluids*, 23 (1996), 1073-1084.
- [28] Anderson, J. D., *Computational Fluid Dynamics - The Basics with Applications*, McGraw-Hill, (1995).
- [29] Ferziger, J. H. and Peric, M., *Computational Methods for Fluid Dynamics*, Springer , (1996).
- [30] Peyret, R. and Taylor, T. D., *Computational Methods for Fluid Flow* , Springer Series in Computational Physics, (1983).
- [31] Fortin, M. and Aboulaich, R., Schwarz's decomposition method for incompressible flow problems, *First International Symposium on Domain Decomposition Methods for Partial Differential Equations*, (1987), 333-349.
- [32] Azaiez, M. and Quarteroni, A., A spectral Stokes solver in domain decomposition methods, *Journal of Contemporary Mathematical*, 180 (1994), 151-156.

Department of Mathematics and Statistics, York University, Toronto, Ontario, M3J 1P3, Canada

E-mail: akhavany@gmail.com

Department of Mathematics and Statistics, York University, Toronto, Ontario, M3J 1P3, Canada

E-mail: chensy@yorku.ca

Department of Mathematics and Statistics, York University, Toronto, Ontario, M3J 1P3, Canada

E-mail: dliang@yorku.ca